Fluorescence Enhancement by Supramolecular Sequestration of a C_{54}-Nanographene Trisimide by Hexabenzocoronene

Bartłomiej Pigulski,[a] Kazutaka Shoyama,[a,b] Meng-Jia Sun,[b] Frank Würthner[a,b,*]
[a]Institut für Organische Chemie, Universität Würzburg, Am Hubland, 97074 Würzburg, Germany
[b]Center for Nanosystems Chemistry (CNC), Universität Würzburg, Theodor-Boveri-Weg, 97074 Würzburg, Germany
Supporting Information Placeholder

ABSTRACT: A supramolecular trilayer nanographene complex consisting of a newly synthesized D_{3h}-symmetric C_{54}-nanographene trisimide (NTI **1**) and two hexabenzocoronenes (**HBC**) has been obtained by self-assembly. This 1:2 complex is structurally well-defined according to NMR and single crystal X-ray studies and exhibits high thermodynamic stability even in polar halogenated solvents. Complexation of NTI **1** by two **HBC** molecules protects the NTI **1** π-surface efficiently from oxygen quenching, thereby leading to a sequestration-induced fluorescence enhancement under ambient conditions.

The design of well-defined supramolecular complexes constitutes a prominent field of research that has been spear-headed by coordinative bonding,[1–3] hydrogen-bonding[4,5] and π–π-stacking interactions.[6,7] However, different from the former two intermolecular forces, most examples for π–π-stacked supramolecular complexes consist of only one type of molecules, i.e. homo-aggregates, and are typically either small-sized dimers or polydisperse large oligomers.[8] Due to a lack of directionality of dispersion forces, these π-stacked structures may suffer from conformational inhomogeneity and for this reason are not necessarily good model systems for the highly important solid state optoelectronic materials based on π-conjugated molecules. However, as we could recently show,[9] this critical situation can be overcome by larger sized polycyclic aromatic hydrocarbons (PAH), also called nanographenes,[10,11] because of the significant gain in binding strength between π-systems upon enlargement of the π-surface.[12] We conjectured that by using high-symmetry π-scaffolds[13–16] and suitably designed bulky substituents[9] well-defined and strongly bound 1:2 complexes of two different PAHs could be produced. Here we describe the synthesis of a new D_{3h}-symmetric C_{54}-nanographene trisimide (NTI **1**) equipped with three bulky imide moieties that can encompass exactly two equivalents of the same D_{3h}-symmetric hexabenzocoronenes (**HBC**, 2,8,14-trimesitylhexabenzo[*bc,ef,hi,kl,no,qr*]coronene). Our studies demonstrate that this trilayer nanographene architecture possesses high structural and thermodynamic robustness. Most importantly, we could observe a sequestration-induced fluorescence enhancement for NTI **1** upon binding of two **HBC** molecules on its top and bottom π-surface which could be rationalized by the sequestration of NTI **1** against oxygen quenching. This is the first demonstration of functional control in such complexes and demonstrates the usefulness of well-defined π-complexes for the elucidation of functional materials properties.

Our synthesis of D_{3h}-symmetric C_{54}-nanographene **1** started from unsubstituted coronene (Scheme 1). In order to synthesize tri-borylated coronene, we used freshly recrystallized $[Ir(OMe)cod]_2$ as a source of iridium,[17,18] 4,4'-dmbpy (4,4′-dimethyl-2,2′-dipyridyl) as a ligand, ^{t}BuOK as a base and cyclohexane as a solvent and succeeded in preparing boronic ester **2** in 21% isolated yield. Next, three-fold [3+3] annulation of **2** with naphthalene imide **3**[19] was carried out. Bulky imide substituents were selected in order to prevent the aggregation of the final product **1**. The reaction of **2** and **3** using $[Pd_2(dba)_3]\cdot CHCl_3$ as palladium source, $PCy_3\cdot HBF_4$ as ligand, Cs_2CO_3 as base and 1-chloronaphthalene as solvent at 180 °C for 2 days gave **1** in 31% isolated yield.

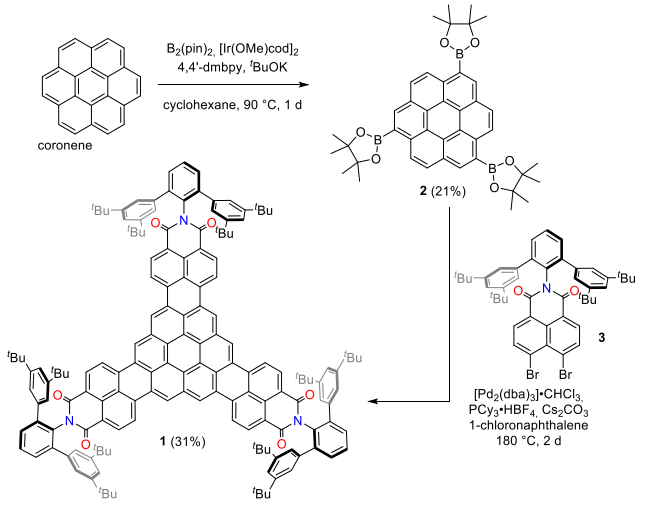

Scheme 1. Synthesis of D_{3h}-symmetric nanographene **1**; cod: 1,5-cyclooctadiene, dba: dibenzylidenoacetone, pin: pinacolato, 4,4'-dmbpy: 4,4′-dimethyl-2,2′-dipyridyl, Cy: cyclohexyl.

Despite of the bulky imide substituents, a strong driving force for aggregation of NTI **1** is evident from the ^{1}H NMR spectrum in CD_2Cl_2. As shown in Figure S28 (Supporting Information), two sets of signals are revealed for the protons of the 3,5-di-*tert*-butylphenyl groups with a 1:1 ratio. The fact that two sets of sharp signals are observed indicates the presence of a defined dimeric structure and a slow exchange on the NMR time-scale due to strong π–π-interactions between the extended C_{54}-nanographene π-scaffolds.[20,21] Upon addition of TFA-*d* (deuterated trifluoroacetic acid) dissociation into monomers took place and only one set of signals from 3,5-di-*tert*-butylphenyl groups was observed. DOSY NMR measurements were performed (SI, Figures S33-34) and diffusion coefficients as well as hydrodynamic radii were determined for the monomeric (D = 4.51×10^{-10} m^2 s^{-1}; r = 11.7 Å) and the dimeric (D = 3.93×10^{-10} m^2 s^{-1}; r = 13.4 Å) state.

The dimerization of NTI **1** was studied in detail by concentration-dependent UV/Vis absorption spectroscopy at 22 °C in CCl_4 (Figure S9), $CHCl_3$ (Figure S10) and CH_2Cl_2 (Figure S11). In each case the diluted samples exhibit two sharp absorption peaks that are located at 548 nm (ε = 1.81×10^5 $M^{-1}cm^{-1}$) and at 512 nm (ε = 1.02×10^5 M^{-1} cm^{-1}) in CH_2Cl_2. Upon increasing concentration the extinction coefficient of the main absorption band drops and both absorption maxima are slightly red-shifted. The whole data sets were globally fitted to the dimerization model to give dimerization constants of 9.44×10^3 M^{-1} ($CHCl_3$), 1.54×10^5 M^{-1} (CH_2Cl_2), and 1.11×10^5 M^{-1} (CCl_4). Because halogenated solvents are known as the best solvents for the solubilization of aromatic π-scaffolds[22] these values are very high and it is accordingly not surprising that similar studies in methylcyclohexane (MCH) could only be performed at elevated temperatures, thereby affording a dimerization constant of 1.7×10^7 M^{-1} at 80 °C (Figure S12).

Next we performed UV/Vis (Figure 1) and fluorescence (SI, Figure S24) titration experiments with hexabenzocoronene (**HBC**) possessing three solubilizing mesityl groups.[23] It is worth to note that **HBC** has the same symmetry as **1** (D_{3h}) and that the choice of the mesityl groups was intended to precisely control the structure of the supramolecular complex by interdigitating the side chains of the guest and host. In the following measurements, diluted solutions of NTI **1** in $CHCl_3$ (concentrations at which only monomeric state is present in solution) were used in order to avoid a competition between dimerization and host–guest complexation. UV/Vis absorption spectra of **1** upon addition of **HBC** showed a significant red-shift and a decrease of the extinction coefficient (Figure 1a). Interestingly, although the emission spectra (Figure S24) also showed bathochromic shift upon addition of **HBC**, they still preserved clearly visible vibronic structure. Both absorption and fluorescence titration data could be fitted globally to the 1:2 binding model (Figure 1b, S25),[24] indicating the formation of a 1:2 complex at the end of the titration. The first (K_1) and second (K_2) binding constants determined from both UV/Vis (K_1 = 1.7×10^5 M^{-1}; K_2 = 4.2×10^4 M^{-1}) and fluorescence (K_1 = 2.4×10^5 M^{-1}; K_2 = 3.3×10^4 M^{-1}) titration experiments are consistent and indicative for a rather independent binding on both π-faces. Importantly, K_1 is almost twenty times higher than the dimerization constant of **1** in $CHCl_3$ which corresponds to an increase of the Gibbs energy by 7.5 $kJmol^{-1}$ that might arise from an enlarged π–π-contact surface (dispersion interaction) or a better electronic complementarity (electrostatics, charge transfer).

Structural proof for the dimer of **1** and the 1:2 complex between **1** and **HBC** was obtained by single crystal X-ray analysis. The X-ray structure reveals isolated dimers in the crystalline state that fully support our earlier studies in solution (Figure 2). Two molecules of **1** are slightly tilted and the whole dimer has a low C_1 symmetry in the solid state (Figure 2c). Space-filling model in Figure 2b clearly show the very tight arrangement of the imide substituents in the dimer. Clearly, there is no space available for a third molecule of **1** to approach from the other side and thus the formation of longer columns is effectively prohibited.

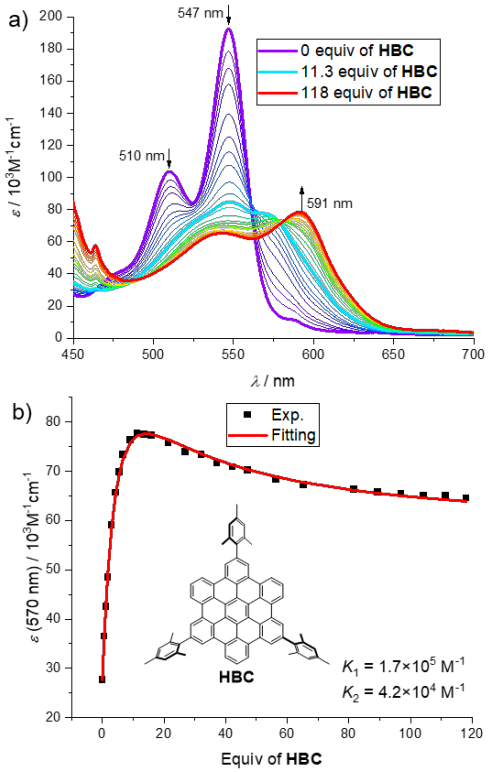

Figure 1. a) UV/Vis titration of host NTI **1** using **HBC** as guest (c_{host} = 1.41×10^{-6} M, $CHCl_3$, 22 °C). b) Global fit to the 1:2 binding model and the experimental values at 570 nm.

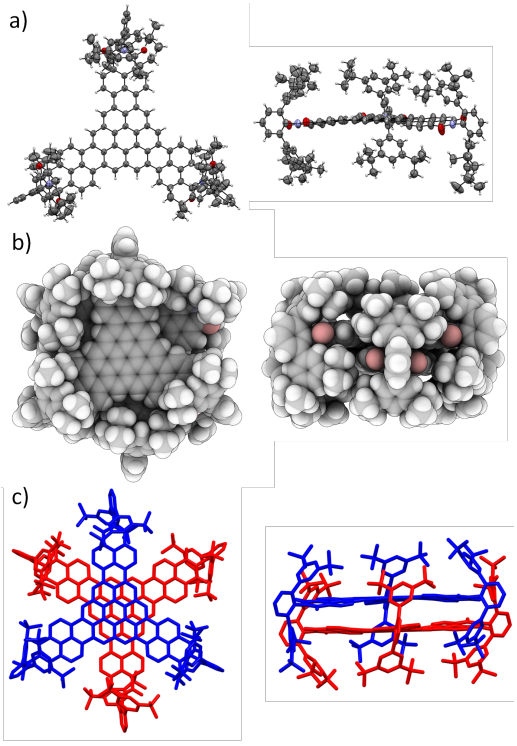

Figure 2. a) Crystal structure of NTI **1** (form A, thermal ellipsoids set at 50% probability). Solvent molecules, hydrogen atoms and disorder of imide substituents were omitted for clarity. b) Space-filling representation of the dimer of **1** in top-(left) and side-view (right). c) Wireframe representation of the dimer of **1**.

Single crystals of the **1**·2(**HBC**) complex were obtained by slow diffusion of *n*-hexane into $CHCl_3$ solution containing **1** and a ten-fold excess of **2**. The X-ray structure confirms the formation of **1**·2(**HBC**) complex suggested from UV/Vis and fluorescence titrations (Figure 3). This triple layer nanographene complex is surrounded by solvent molecules and does not form extended columnar π-stacks in the solid state. All three π-surfaces are slightly tilted and the whole trilayer structure adopts a low C_1 symmetry in the solid state. The π-π contact surface (SI, Figures S4, S5) between **1** and **HBC** molecules (78 $Å^2$) is increased compared to one in the dimer of **1** (62 $Å^2$), which might explain the higher binding affinity for the **HBC** complex simply by dispersion forces.

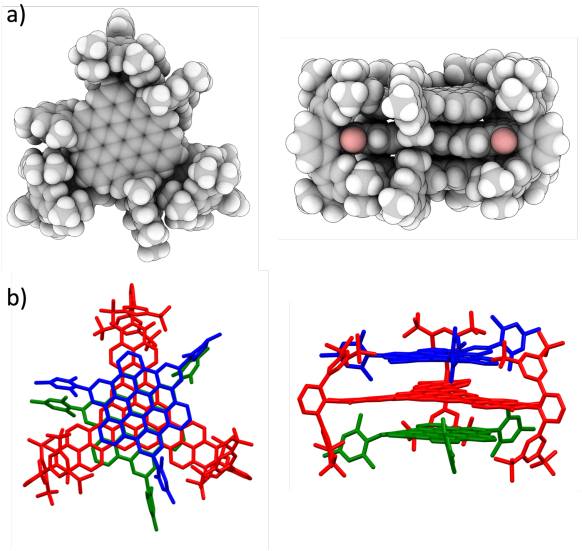

Figure 3. Molecular structure of **1**·2(**HBC**) complex from X-ray single crystal analysis. a) Space-filling representation in top- (left) and side-view (right). b) Wireframe representation with molecule **1** in red and two independent **HBC** molecules in green and blue in top- (left) and side-view (right); hydrogen atoms and solvent molecules removed for clarity.

Fluorescence measurements of monomeric NTI **1** were conducted using its diluted chloroform solutions (Figure 4a). A large Stokes shift ($\Delta\nu$ = 2800 cm^{-1}) could be observed that is explained by the forbidden character of the $S_0 \rightarrow S_1$ transition (SI, Table S2). Despite this forbidden $S_0 \rightarrow S_1$ transition, the fluorescence quantum yield is rather high (Φ_{FL} = 12.5 ± 1.7% in $CHCl_3$, Figure 4c, Table S4). This interesting behavior is due to an unusually long fluorescence lifetime of **1** (τ = 34.0 ns in $CHCl_3$, Figure 4b) compared to other bis- or multiimides. The fluorescence of dimeric **1** (Figure S18) measured in MCH is much weaker (Φ_{FL} = 6.0 ± 0.8%), and has structureless excimer-like shape and a similar lifetime (τ_{avg} = 27.1 ns) as monomeric NTI **1**.

The fluorescence of **1**·2(**HBC**) complex was analyzed in more detail. Usually for comparable systems lower quantum yields and structureless exciplex-like emission are reported.[9,25] However, the quantum yield of **1**·2(**HBC**) was significantly higher (Φ_{FL} = 21.2 ± 0.6%) than for pure **1** in $CHCl_3$ (Φ_{FL} = 12.5 ± 1.7%) and vibronic structure of an emission band was preserved indicating lack of charge transfer character.[26] Vibronic progression ($\Delta\upsilon$ ~ 1300 cm^{-1}) and Stokes shift ($\Delta\upsilon$ ~ 2400 cm^{-1}) of **1**·2(**HBC**) were also very similar to that of **1** but its fluorescence lifetime is significantly longer (τ_{avg} = 49.8 ns). To get additional insight into this phenomenon we conducted fluorescence measurements under oxygen-free conditions since oxygen is known as an efficient quencher of luminescence of PAHs.[27,28] Whilst the shape of emission and excitation spectra of all investigated species were not influenced by the presence of oxygen, we indeed observed a significant increase of the fluorescence quantum yield of monomeric NTI **1** to 24.5 ± 1.7% as well as an increase of the fluorescence decay time to 53.5 ns. In contrast, the fluorescence enhancement of **1**·2(**HBC**) complex was negligible (from 21.2 ± 0.6% to 26.7 ± 1.6%) and likewise the increase of the fluorescence decay time remained modest (67.7 ns).

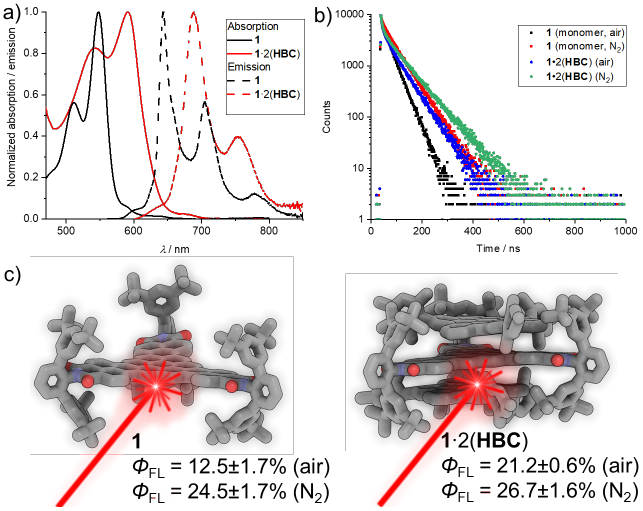

Figure 4. a) Emission (dashed) and absorption (solid) spectra of monomeric **1** (c ~ 10^{-7} M, ex.: 550 nm) and **1**·2(**HBC**) in $CHCl_3$ (c ~ 10^{-7} M, ex.: 590 nm) in air at 22 °C; b) Fluorescence decay of **1** ($CHCl_3$, air: τ_{avg} = 34.0 ns, N_2:, τ_{avg} = 53.5 ns) and **1**·2(**HBC**) ($CHCl_3$, air: τ_{avg} = 49.8 ns, N_2: τ_{avg} = 67.7 ns) at 22 °C; c) Absolute fluorescence quantum yields of monomeric **1** and **1**·2(**HBC**) in $CHCl_3$.

Our explanation for the improved fluorescence of NTI **1** by complexation with two **HBC** molecules is accordingly, that the **HBC** molecules sequester NTI **1** from diffusion-controlled encounters with oxygen that like for other PAHs[27,28] leads to an additional non-radiative decay channel. This conclusion is supported by the ratio of radiative (k_r) and nonradiative (k_{nr}) decay rates (Table S5) which is over two times higher for monomeric **1** (0.32) measured under inert atmosphere than for **1** measured in the presence of oxygen (0.14) but is similar to **1**·2(**HBC**) measured in the presence of air (0.27). The increase of k_r/k_{nr} ratio for **1**·2(**HBC**) measured under inert conditions is in contrast significantly smaller (from 0.27 to 0.36) We note here rigidification as another minor contribution to the enhancement of fluorescence upon complexation because the nonradiative decay constant measured under oxygen-free conditions is slightly decreased for **1**·2(**HBC**) (k_{nr} = 1.1×10^{-2} ns^{-1}) compared to **1** (k_{nr} = 1.4×10^{-2} ns^{-1}) (SI, Table S5).

In summary, we presented a well-defined tightly packed self-assembled nanographene trilayer structure consisting of a newly designed D_{3h}-symmetric nanographene trisimide emitter **1** that is sandwiched by two hexabenzocoronenes. The complimentary molecular shape of this D_{3h}-nanographene and hexabenzocoronene guest enabled a perfect sequestration of the functional unit **1** within a supramolecular π-stack **1**·2(**HBC**). Complex **1**·2(**HBC**) exhibits stronger and more long-lived fluorescence than monomer **1** in the presence of air due to prevention of diffusional encounters with oxygen. The large Stokes shift combined with relatively high fluorescence quantum yield of **1**·2(**HBC**) complex illustrates a new approach toward highly fluorescent materials with reduced reabsorption as required for advanced light harvesting systems, e.g. in luminescent solar

concentrators.[29,30] We anticipate that this well-characterized trilayer nanographene system will motivate further research in the development of multilayer nanographenes with precisely controlled structure and function.

ASSOCIATED CONTENT

Supporting Information

The Supporting Information is available free of charge on the ACS Publications website.
Synthesis of all new compounds, UV/Vis, fluorescence, NMR and mass spectra, details of X-ray diffraction experiments. (PDF).

Accession Codes

CCDC 2025782–2025784 contain the supplementary crystallographic data for this paper. These data can be obtained free of charge via www.ccdc.cam.ac.uk/data_request/cif, or by emailing data_request@ccdc.cam.ac.uk, or by contacting The Cambridge Crystallographic Data Centre, 12 Union Road, Cambridge CB2 1EZ, UK; fax: +44 1223 336033

AUTHOR INFORMATION

Corresponding Author

wuerthner@uni-wuerzburg.de
ORCID
Bartłomiej Pigulski 0000-0002-9925-2878
Kazutaka Shoyama 0000-0003-0937-4431
Meng-Jia Sun 0000-0001-8117-9257
Frank Würthner 0000-0001-7245-0471

Present Addresses

Bartłomiej Pigulski: Faculty of Chemistry, University of Wrocław, 14 F. Joliot-Curie, 50-383 Wrocław, Poland.

Notes

The authors declare no competing financial interests.

ACKNOWLEDGMENT

The authors are grateful for financial support from the Deutsche Forschungsgemeinschaft (DFG) (Grant Wu 317/20-2). We acknowledge DESY (Hamburg, Germany), a member of the Helmholtz Association HGF, for providing experimental facilities at PETRA III. We thank Mateusz Mieczkowski and Claudia Höbartner for sharing measurement time under P11 proposal No I-20190778, and we thank Sofiane Saouane for assistance in using beamline P11.

REFERENCES

[1] Lehn, J.-M.*; Supramolecular Chemistry: Concepts and Perspectives*, Wiley-VCH, 1995.
[2] Fujita, M.; Tominaga, M; Hori, A., Coordination assemblies from a Pd(II)-cornered square complex. *Acc. Chem. Res.* 2005, **38**, 369-378.
[3] Sun, Y.; Chen, C. Y.; Liu, J. B.; Stang, P. J., Recent developments in the construction and applications of platinum-based metallacycles and metallacages via coordination. *Chem. Soc. Rev.* **2020**, *49*, 3889-3919.
[4] Prins, L. J.; Reinhoudt, D. N.; Timmerman, P., Noncovalent synthesis using hydrogen bonding. *Angew. Chem. Int. Ed.* **2001**, *40*, 2382-2426.
[5] Hof, F.; Craig, S. L.; Nuckolls, C.; Rebek, J., Molecular encapsulation. *Angew. Chem. Int. Ed.* **2002**, *41*, 1488-1508.
[6] Hunter, C. A.; Meldola Lecture – The role of aromatic interactions in molecular recognition. *Chem. Soc. Rev.* **1994**, *23*, 101-109.
[7] Chen, Z.; Lohr, A.; Saha-Möller, C. R.; Würthner, F., Self-assembled π-stacks of functional dyes in solution: structural and thermodynamic features. *Chem. Soc. Rev.* **2009**, *38*, 564–584.
[8] Bialas, D.; Kirchner, E.; Röhr, M.; Würthner, F., Perspectives in Dye Chemistry: A Rational Approach toward Functional Materials by Understanding the Aggregate State. *J. Am. Chem. Soc.* **2021**, *143*, 4500-4518.
[9] Mahl, M.; Niyas, M. A.; Shoyama, K.; Würthner, F., Multilayer stacks of polycyclic aromatic hydrocarbons. *Nat. Chem.* **2022**, doi: 10.1038/s41557-021-00861-5.
[10] Narita, A.; Wang, X.-Y.; Feng, X.; Müllen, K., New advances in nanographene chemistry. *Chem. Soc. Rev.* **2015,** *44* (18), 6616-6643.
[11] Stępień, M.; Gońka, E.; Żyła, M.; Sprutta, N., Heterocyclic Nanographenes and Other Polycyclic Heteroaromatic Compounds: Synthetic Routes, Properties, and Applications. *Chem. Rev.* **2017,** *117* (4), 3479-3716.
[12] Grimme, S., Do special noncovalent π-π stacking interactions really exist? *Angew. Chem. Int. Ed.* **2008**, *47*, 3430-3434.
[13] Pho, T. V.; Toma, F. M.; Chabinyc, M. L.; Wudl, F., Self-Assembling Decacyclene Triimides Prepared through a Regioselective Hextuple Friedel–Crafts Carbamylation. *Angew. Chem. Int. Ed.* **2013,** *52* (5), 1446-1451.
[14] Pozo, I.; Guitián, E.; Pérez, D.; Peña, D., Synthesis of Nanographenes, Starphenes, and Sterically Congested Polyarenes by Aryne Cyclotrimerization. *Acc. Chem. Res.* **2019,** *52* (9), 2472-2481.
[15] Feng, X.; Wu, J.; Ai, M.; Pisula, W.; Zhi, L.; Rabe, J. P.; Müllen, K., Triangle-Shaped Polycyclic Aromatic Hydrocarbons. *Angew. Chem. Int. Ed.* **2007,** *46* (17), 3033-3036.
[16] Zhang, Q.; Peng, H.; Zhang, G.; Lu, Q.; Chang, J.; Dong, Y.; Shi, X.; Wei, J., Facile Bottom-Up Synthesis of Coronene-based 3-Fold Symmetrical and Highly Substituted Nanographenes from Simple Aromatics. *J. Am. Chem. Soc.* **2014,** *136* (13), 5057-5064.
[17] Eliseeva, M. N.; Scott, L. T., Pushing the Ir-Catalyzed C–H Polyborylation of Aromatic Compounds to Maximum Capacity by Exploiting Reversibility. *J. Am. Chem. Soc.* **2012,** *134* (37), 15169-15172.
[18] Ji, L.; Fucke, K.; Bose, S. K.; Marder, T. B., Iridium-Catalyzed Borylation of Pyrene: Irreversibility and the Influence of Ligand on Selectivity. *J. Org. Chem.* **2015,** *80* (1), 661-665.
[19] Mahl, M.; Shoyama, K.; Krause, A.-M.; Schmidt, D.; Würthner, F., Base-Assisted Imidization: A Synthetic Method for the Introduction of Bulky Imide Substituents to Control Packing and Optical Properties of Naphthalene and Perylene Imides. *Angew. Chem. Int. Ed.* **2020,** *59* (32), 13401-13405.
[20] Zhao, X.-J.; Hou, H.; Fan, X.-T.; Wang, Y.; Liu, Y.-M.; Tang, C.; Liu, S.-H.; Ding, P.-P.; Cheng, J.; Lin, D.-H.; Wang, C.; Yang, Y.; Tan, Y.-Z., Molecular bilayer graphene. *Nat. Commun.* **2019,** *10* (1), 3057.
[21] Matsumoto, I.; Sekiya, R.; Haino, T., Self-Assembly of Nanographenes. *Angew. Chem. Int. Ed.* **2021**, *60*, 12706-12711.
[22] Würthner, F., Solvent Effects in Supramolecular Chemistry: Linear Free Energy Relationships for Common Intermolecular Interactions. *J. Org. Chem.* **2022**, *87* (3), 1602–1615.
[23] Cui, S.; Zhuang, G.; Lu, D.; Huang, Q.; Jia, H.; Wang, Y.; Yang, S.; Du, P., A Three-Dimensional Capsule-like Carbon Nanocage as a Segment Model of Capped Zigzag [12,0] Carbon Nanotubes: Synthesis, Characterization, and Complexation with C_{70}. *Angew. Chem. Int. Ed.* **2018,** *57* (30), 9330-9335.
[24] Thordarson, P., Determining association constants from titration experiments in supramolecular chemistry. *Chem. Soc. Rev.* **2011,** *40* (3), 1305-1323.
[25] Birks, J. B., Excimers and Exciplexes. *Nature* **1967,** *214* (5094), 1187-1190.
[26] Das, A.; Ghosh, S. Supramolecular Assemblies by Charge-Transfer Interactions between Donor and Acceptor Chromophores. *Angew. Chem. Int. Ed.* **2014**, *53*, 2038-2054.
[27] Ware, W. R. Oxygen Quenching Of Fluorescence In Solution: An Experimental Study Of The Diffusion Process *J. Phys. Chem.* **1962**, *66*, 455–458.
[28] Okamoto, M.; Tanaka, F. Quenching by Oxygen of the Lowest Singlet and Triplet States of Pyrene and the Efficiency of the Formation of Singlet Oxygen in Liquid Solution under High Pressure *J. Phys. Chem. A* **2002**, *106* (15), 3982–3990.
[29] Debije, M. G. Solar Energy Collectors with Tunable Transmission, *Adv. Funct. Mater.* **2010**, *20*, 1498-1502.
[30] Meinardi, F.; Bruni, F.; Brovelli, S. Luminescent solar concentrators for building-integrated photovoltaics. *Nat. Rev. Mater.* **2017**, *2*, 17072.

TOC